Strongly confined gap plasmon modes in graphene sandwiches and graphene-on-silicon

2013 New J. Phys. 15 063020

(http://iopscience.iop.org/1367-2630/15/6/063020)

New Journal of Physics
The open access journal for physics

Strongly confined gap plasmon modes in graphene sandwiches and graphene-on-silicon

Yan Francescato[1], **Vincenzo Giannini and Stefan A Maier**
The Blackett Laboratory, Imperial College London, London SW7 2AZ, UK
E-mail: yan.francescato10@imperial.ac.uk

New Journal of Physics **15** (2013) 063020 (13pp)
Received 28 February 2013
Published 14 June 2013
Online at http://www.njp.org/
doi:10.1088/1367-2630/15/6/063020

Abstract. We explore the existence of tightly confined gap modes in structures consisting of two infinitely long graphene ribbons vertically offset by a gap. By investigating carefully such a sandwich geometry we find that the gap modes originate from a strong hybridization that gives rise to improved waveguide performance while modifying the guiding behaviour compared to a single ribbon. Our work particularly focuses on the physical origin and description of these plasmon modes, studying the critical parameters of width, gap and operation wavelength. This allows different regimes, coupling mechanisms and mode families to be recognized. Importantly we show that the gap modes also exist when a single graphene sheet is placed on top of a metal or a doped semiconductor—a geometry that is readily achievable experimentally. As an example we report on an unprecedented level of confinement of a terahertz wave of nearly five orders of magnitude when a graphene ribbon is placed on top of a highly doped silicon substrate. Because of their remarkable field distributions and extreme confinement, the families of modes presented here could be the building blocks for both graphene-based integrated optics and ultrasensitive sensing modalities.

[1] Author to whom any correspondence should be addressed.

Contents

1. Introduction

Since its discovery, graphene has emerged as a radically new platform for nanoscience and condensed matter physics in general [1]. A truly two-dimensional crystal [2] with tunable properties, the full potential of graphene is just being unveiled [3, 4]. In nanophotonics and optoelectronics for instance [5–8], both intraband and interband processes can be engineered from the terahertz range, where functional materials are sparse [9–12], to the visible, making graphene an appealing candidate to supplant metals and semiconductors, respectively. Indeed the carrier concentration and the Fermi level are easily modified through chemical doping [13] or electrostatic gating [14–18], and optical injection [19] is also possible, paving the way towards active ultrafast control of the graphene response. Another key component is the ability to confine electromagnetic waves below the diffraction limit in order to obtain high local field enabling nonlinearities and small lateral spreading for integrated optics. Conceptually similar to SPPs in metals, in graphene these oscillations of the surface charge coupled to the electromagnetic field exhibit unusually strong confinement compared to the former [20–22]. With sufficient doping there is even the prospect of operation in the telecom wavelength regime [23].

In order to further engineer the plasmonic response of graphene, for applications as electromagnetic waveguides similar to what has been done over the past decade with metallic nanostructures [24], geometry-induced confinement is possible [25–37]. For instance, nanoribbons can readily be fabricated by current e-beam technology and measurements of plasmonic resonances were recently reported [16–18]. Theoretically, Nikitin *et al* [38] studied thoroughly single ribbons and showed they exhibit typical plasmonic waveguide modes with cut-off frequencies depending on the ratio between wavelength and width, similar to the modes supported by metallic stripes for instance [39]. Graphene ribbons also support very localized modes travelling along the edges [38] which derive from the corner modes in plasmonic waveguides in the limit of vanishing thickness [39]. Paired ribbons were then considered by Christensen *et al* revealing an even richer mode spectrum caused by lift of degeneracy and hybridization [40]. However, in contrast to previous works we are concerned with identifying simple configurations which can be easily realized in experiments and effective way to describe the performances of these modes. We investigate

here the full range of gap sizes, operation wavelengths and ribbon widths presenting a complete overview of the coupled modes in graphene sandwiches including bonding and anti-bonding waveguide modes. Highlighting the physics of the hybridization in these systems we are able to conceive realistic and highly promising designs utilizing even a single ribbon placed at a distance from a conductive plane, as will be shown in this paper. Our study conclusively identifies the parameter space available for a graphene waveguide-lead technology.

In the present study, we analyse infinitely long graphene nanoribbons placed on top of each other and separated by a gap, a sandwich geometry. First of all, we introduce a new approach to represent graphically the mode spectrum highlighting at the same time both the propagation of the mode and its confinement. This proves to be ideally suited to distinguish different families of modes sharing similar dispersion characteristics, and also simplifies their visualization in case of high mode densities. Subsequently, we vary the width of the ribbons as well as the wavelength of the incident light in order to sweep across the waveguide regime cut-off and as a result notice the emergence of additional modes. More specifically, these modes can be associated with symmetric and antisymmetric coupling of the isolated ribbon spectra. Analysing carefully this hybridization with decreasing gap we observe different coupling mechanisms for waveguide and edge modes, depending on their symmetries. Furthermore, it is shown that the resulting coupled graphene sandwich always exhibits improved performance compared to the single ribbon, as well as a modified cut-off behaviour. Some simple analytical relations allow one to easily estimate the necessary doping at a given operation wavelength for optimum propagation and single-mode regime, as well as determining the modal cut-off—essential ingredients in any waveguide-based technology. Lastly, we demonstrate that similar modes are also supported by more easily achievable systems, where a single graphene ribbon is placed on top of a conducting substrate with a gap filled by a dielectric spacer. Remarkably, such a configuration conserves the gap modes and promises high confinement of nearly five orders of magnitude in the terahertz regime. From their very specific field distributions and extraordinary confinement we also elucidate the advantages offered by each family of modes regarding concrete applications such as sensing and nanocircuitry.

2. Classification of mode families

Before presenting the complex mode spectra of strongly coupled graphene nanoribbons, let us first introduce the graphical convention used throughout this paper, and recall the modes that exist in a single ribbon infinitely long in the Y-direction and of width W, shown schematically in figure 1(a).

We consider here typical values for doped graphene with a chemical potential $\mu = 0.5\,\mathrm{eV}$ and a charge carrier scattering rate $\Gamma = 0.1\,\mathrm{meV}$, described by a complex permittivity (see the appendix) [38]. If we consider a wide graphene nanoribbon (see figure 1(a)), it has been shown that this waveguide system can support two kinds of plasmon modes: on the one hand, edge modes with very high one-dimensional confinement and on the other hand, typical waveguide modes with cut-off frequencies depending on the ratio between wavelength and width as well as the mode order [38]. Both types of mode are travelling along the Y-direction, with the waveguide mode exhibiting a standing wave across the width and the edge mode having a field distribution located close to the border of the ribbon. With each of these modes one can associate a complex propagation constant $q = k_\mathrm{p}/k_0$, with $k_0 = 2\pi/\lambda_0 = \omega/c$ the wavevector of light in

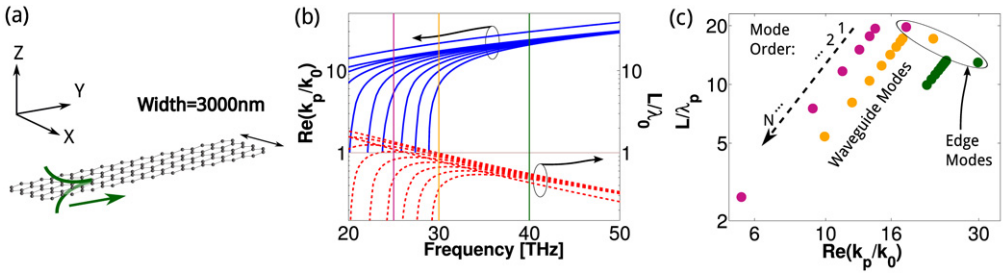

Figure 1. (a) Axis convention and geometry of the considered graphene ribbon with a chemical potential $\mu = 0.5\,\mathrm{eV}$ and charge carrier scattering rate $\Gamma = 0.1\,\mathrm{meV}$. (b) Normalized wavevector $\Re(k_\mathrm{p}/k_0)$ (blue lines) of the modes and propagation length L/λ_0 (red dashed curves) in log scale versus the frequency for a 3000 nm wide graphene nanoribbon. (c) The same modes as in (b) at 25 (violet), 30 (orange) and 40 THz (green) plotted as L/λ_p versus $\Re(k_\mathrm{p}/k_0)$ on a log–log scale.

vacuum, which describes the wavelength of the guided plasmon mode $\lambda_\mathrm{p} = 2\pi/k_\mathrm{p} = \lambda_0/\Re(q)$ and its propagation length $L = \lambda_0/4\pi\Im(q)$ defined as the $1/e$ intensity decay length of the plasmon along its propagation direction. Traditionally, such a spectrum is plotted as shown in figure 1(b), here for the case of a $W = 3000\,\mathrm{nm}$ wide ribbon in the range 20–50 THz ($\lambda_0 = 15 - 6\,\mu\mathrm{m}$), with the normalized wavevector $\Re(q)$ (blue curves) and the normalized propagation length L/λ_0 (red dashed lines) plotted separately versus the frequency [38, 41]. One can recognize the sharp decrease in the wavevector and the propagation of the mode when it approaches cut-off. This modal cut-off means that as the frequency (or the width) decreases, the group velocity slows down, causing a significant rise in the dissipation until the mode stops propagating completely.

Since the decay of the modes is such a crucial property ultimately determining their usefulness, we propose an alternative representation, selecting single frequencies, and plotting the normalized propagation L/λ_p versus the normalized wavevector $\Re(q)$ on a log–log scale, see figure 1(c) for 25 (12), 30 (10) and 40 THz ($\lambda_0 = 7.5\,\mu\mathrm{m}$). In this manner, one can easily distinguish between the waveguide modes distributed along a line and the edge modes set a bit apart at higher wavevectors. Low order modes are located at high wavevectors and propagation lengths and these are simultaneously decreased when the order of the mode increases. We will see later that this representation is also very instructive when coupling occurs in multilayers, because the mode density increases considerably and it gets possible to follow their behaviour simply by considering a single slice of the dispersion diagram, i.e. looking at one frequency at a time, grouping the modes by families. The propagation compared to λ_0 is also easily accessible by dividing L/λ_p by its abscissa, $\Re(q)$. Last, the confinement of the plasmon within the surrounding medium $\delta/\lambda_0 = k_0/4\pi\Im(k_z)$, even though not included, is very similar in magnitude to $1/4\pi\Re(q)$; indeed, since $k_\mathrm{p} \gg k_0$, $k_z = \sqrt{k_0^2 - k_\mathrm{p}^2} \sim \mathrm{i}k_\mathrm{p}$ which means that $\Im(k_z) \approx \Re(k_\mathrm{p})$. Note as expected that these relations imply that for a given system and mode order, a tighter confinement leads to a reduced propagation length and vice versa (see figures 1(b) and (c)).

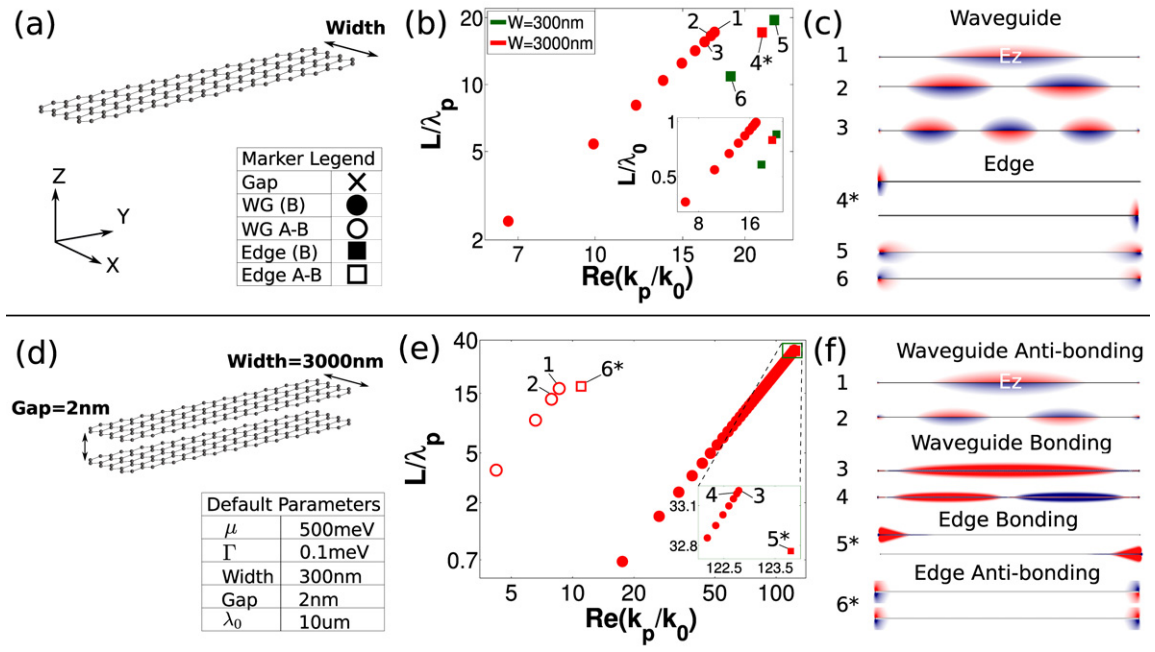

Figure 2. (a) Ribbon geometry and symbols convention. (b) Mode spectrum of 300 nm (green) and 3000 nm (red) graphene ribbons at $\lambda_0 = 10\,\mu$m; the inset shows the same modes with the propagation length normalized to the free space wavelength. (c) E_z field with positive (negative) sign coloured in red (blue) for the modes numbered in (b), the '$*$' denotes the degeneracy of the modes. (d) Sandwich geometry and summary of the default parameters used throughout the paper unless otherwise specified. (e) Mode spectrum exhibited by a sandwich of two 3000 nm wide ribbons vertically offset by 2 nm, the inset is a zoom of the green rectangle in the top right-hand side corner; bonding modes are represented with full markers while anti-bonding ones are marked with open symbols. (f) E_z field of the modes numbered in (e).

3. Results and discussion

3.1. Single versus sandwiched ribbons

Keeping this convention for plotting a mode spectrum, let us now compare the same ribbon with a narrower one with a width small enough to be above the lateral cut-off at $\lambda_0 = 10\,\mu$m (30 THz). A detailed account of the method used to determine this fundamental parameter will be given in the next section. The top panel of figure 2 shows the modes of such a single ribbon above ($W = 300$ nm, green symbols) and below ($W = 3000$ nm, in red) the waveguide cut-off.

One can appreciate how the chosen convention for plotting helps to distinguish easily between the waveguide and edge modes. In order to highlight this even further, we use different symbols for plotting waveguide (circle) and edge (square) modes, see table in figure 2(a). The inset in figure 2(b) shows L/λ_0 rather than L/λ_p for the same structures. On the right-hand side, the field E_z for the first three order waveguide modes (1–3) is shown with positive (negative)

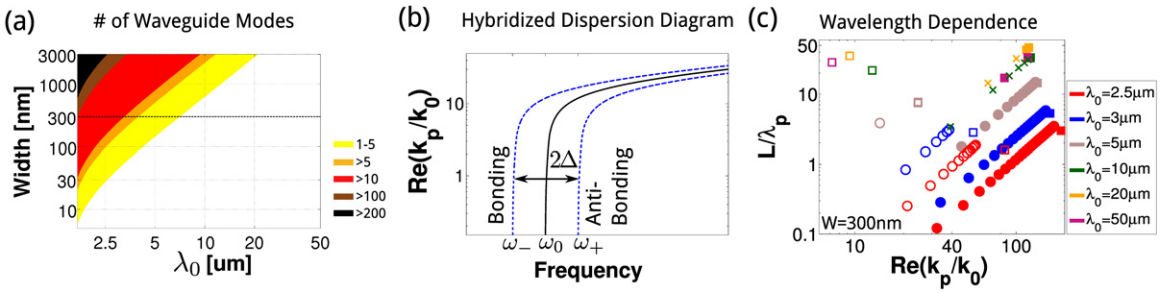

Figure 3. (a) Number of waveguide modes in a single graphene ribbon as given by $N < \frac{2W}{\lambda}[\mathrm{i}\varepsilon_0(\varepsilon_\mathrm{m}+1)c/\sigma - \sqrt{\varepsilon_\mathrm{m}}]$. (b) Schematic of the hybridization mechanism as seen in the dispersion diagram. (c) Mode spectra for a sandwich with 300 nm width and 2 nm gap at different wavelengths; the marker legend is the same than in figure 2(a).

sign coloured in red (blue). When comparing the edge modes, one can see a crucial difference between narrow and wide ribbons. For the latter, there exist two degenerate modes (4*, where the '$*$' denotes the degeneracy of the modes) while the degeneracy is lifted as the ribbon gets narrower (5–6) [38].

If two ribbons with $W = 3000$ nm are placed on top of each others with a gap $G = 2$ nm, the spectrum splits up in bonding (full markers) and anti-bonding (open symbols) modes as shown in the bottom panel of figure 2. Bonding modes have opposite charges across the gap while anti-bonding ones have no field between the two ribbons [42]. This is apparent in the field distributions of the first waveguide (3–4 versus 1–2) and edge modes (5* versus 6*) on the right-hand side. It is also intriguing to note that as the modes of a single ribbon, the bonding and anti-bonding combinations follow the same linear dispersion on a log–log scale.

3.2. Mode evolution

3.2.1. Single ribbon cut-off. The cut-off regime and more generally the number of waveguide modes in a plasmonic stripe can be well estimated from general considerations [41]. Writing all the components of a surface plasmon polaritons (SPPs) with wavevector $\overrightarrow{k} = (k_x, k_y, k_z)$ (see figure 2(a) for the axis convention) we have at a given frequency $(\omega/c)^2\varepsilon_\mathrm{m} = k_0^2\varepsilon_\mathrm{m} = |k|^2 = k_x^2 + k_y^2 + k_z^2$, where ε_m is the permittivity of the medium surrounding the conducting surface. In the electrostatic limit, the in-plane momentum of such SPPs for an infinite graphene sheet reads $k_\mathrm{spp} = \sqrt{k_x^2 + k_y^2} = \mathrm{i}\varepsilon_0(\varepsilon_\mathrm{m}+1)\omega/\sigma$ [23]. It is reasonable to assume that the vertical wavevector k_z is left mostly unaffected by the finite width of the ribbons so that the supported plasmons have an in-plane momentum $\sim k_\mathrm{spp}$. In order for waveguiding to occur $k_y^2 > k_0^2\varepsilon_\mathrm{m}$ which imposes a condition on k_x through $k_x^2 = k_\mathrm{spp}^2 - k_y^2 < k_\mathrm{spp}^2 - k_0^2\varepsilon_\mathrm{m}$. At the same time, the highest order mode supported by the stripe will have N extrema along the width so that $k_{x,\mathrm{max}} = N\pi/W$. Hence it follows that the number of modes in a graphene ribbon is given to a good approximation by $N < \frac{2W}{\lambda}[\mathrm{i}\varepsilon_0(\varepsilon_\mathrm{m}+1)c/\sigma - \sqrt{\varepsilon_\mathrm{m}}]$.

Figure 3(a) shows the number of waveguide modes obtained from this derivation depending on both the width and the operation wavelength for a single graphene ribbon. By comparison with the numerical results we find a very good agreement.

3.2.2. Cut-off in sandwich geometry. If one considers now a sandwich geometry, the hybridization will lead to the formation of anti-bonding and bonding waveguide modes with energies given by $\omega_{\pm} = \omega_0 \pm \Delta$, with ω_0 the single ribbon energy spectrum and Δ the energy shift. This process is schematically presented in figure 3(b) and shows clearly that the cut-off of the bonding (anti-bonding) mode will be redshifted (blueshifted) compared to the original ribbon. It also elucidates that, for a given mode order, while anti-bonding have higher energies than bonding modes, they exhibit smaller wavevectors.

The mode spectrum of a sandwich for the case of 300 nm wide ribbons with a 2 nm gap is presented in figure 3(c). One can see that as the free space wavelength increases towards the cut-off the number of modes gets reduced until ($\lambda_0 \geqslant 50\,\mu$m) only edge modes survive; confirming the intuition provided by figure 3(b) anti-bonding modes do indeed disappear at shorter wavelength than bonding ones. The latter are marked with a cross when still existing above the cut-off of the single ribbon such as at 10 and 20 μm (green and orange symbols in figure 3(c)). Because they have different field profiles than bonding waveguide modes and exist only in a specific regime we will refer to these modes as gap modes in the following. The properties of these modes as well as the conditions for their existence will be the focus of the rest of this paper, along with a detailed study of the hybridization in such a sandwich geometry. From figure 3(c) it can also be concluded that there is an optimum operation wavelength at which propagation losses are minimum, here 20 μm (notice how both edge modes at 10 and 50 μm propagate less than at 20 μm). In fact, this optimum is mostly conserved from the isolated ribbon and is given by the maximum of $\Re(k_{\mathrm{spp}})/\Im(k_{\mathrm{spp}})$. However there is no such an optimum for the confinement, which monotonically decreases as the wavelength increases. Interestingly, the frequency at which the propagation is maximum also corresponds to a regime where there exists only a single or few gap mode in the sandwich.

3.3. Mode hybridization

In order to obtain further insight into the hybridization mechanism we are going to consider the same 300 nm wide sandwich below (at $\lambda_0 = 2.5\,\mu$m) and above cut-off (at $\lambda_0 = 10\,\mu$m) while changing the coupling strength between the two ribbons, namely by modifying the interlayer spacing.

3.3.1. Hybridization below cut-off (supporting waveguide modes). As described in the previous section, when the waveguide modes of two ribbons start to interact, they will combine into either an anti-bonding or a bonding state as shown in figure 4(a).

Investigating the mode spectrum, figure 4(b), two ensembles of modes, anti-bonding (open symbols) and bonding (full markers), at small and large wavevectors, can be clearly distinguished. As the gap is increased, the splitting is reduced until the two set of modes converge at large gap to the spectrum of a single ribbon (in black). A similar behaviour is also observed for the edge modes (squares) as indicated by the dashed line where the gap lifts the degeneracy which exists in the uncoupled structure. There are two major conclusions from figure 4: on the one hand, and as can be expected, when comparing the same mode order the bonding modes of the sandwich geometry always present a stronger confinement (larger $\Re(q)$) than the original ribbon, while anti-bonding modes exhibit longer propagation because of decreased confinement. This means that if the hybridization, or in other words the gap, can be controlled, one has a direct influence on the waveguiding properties of the graphene

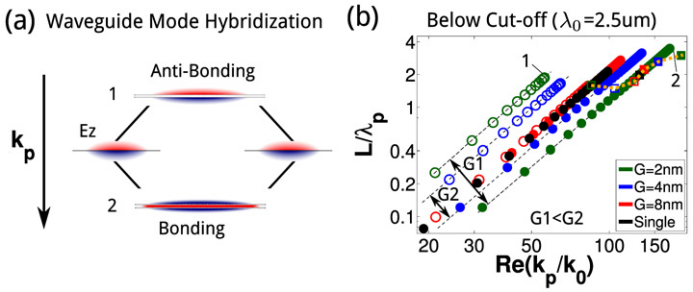

Figure 4. (a) E_z fields and hybridization mechanism between two single ribbon waveguide modes splitting into anti-bonding and bonding combinations. (b) Mode spectra of a graphene sandwich at $\lambda_0 = 2.5\,\mu$m (below cut-off) for different gap sizes (coloured markers) compared with a single ribbon (black symbols), the E_z fields for the numbered modes are shown in (a) and the dashed line indicates the evolution of the edge modes with the gap.

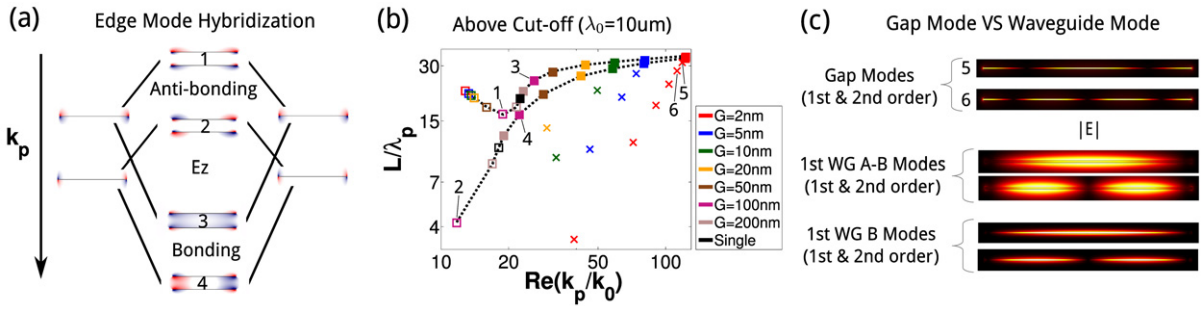

Figure 5. (a) E_z fields and hybridization mechanisms for the symmetric and antisymmetric edge modes in single ribbons when brought in proximity to each others. (b) Mode spectra of a graphene sandwich at $\lambda_0 = 10\,\mu$m (above cut-off) for different gap sizes (coloured markers) compared with a single ribbon (black symbols); the dashed lines indicate the evolution for the two branches of edge modes with different symmetries and the E_z fields for the numbered modes are shown in (a). (c) Difference in the field $|E|$ distribution between gap, anti-bonding and bonding waveguide modes.

nanostructure. On the other hand, it reveals that because of symmetry the interaction only proceeds between modes of the same order in the two ribbons.

3.3.2. Hybridization above cut-off (no waveguide mode). For narrower ribbons, or longer wavelengths, the edges of a single structure are already able to interact lifting the initial degeneracy, as was shown in figures 2(b)–(c) for instance. There, the narrow ribbon exhibits two edge modes (5 and 6) while the wider graphene supports one degenerate mode (4*) [38]. As seen in figure 5(a) (and figure 2(c)) the two resulting edge modes in narrow ribbons have different symmetries and so cannot cross each other. Therefore, in a sandwich, one sees the emergence of four edge modes which can be separated into two sub-families, figure 5(a).

In the mode spectrum, these two categories of edge modes will evolve as different branches, as can be seen in figure 5(b) (and also figure 3(c)). For small gaps, the edge mode of lowest symmetry (2) is disappearing while the two bonding states merge (3 and 4). Of particular interest is the existence of bonding waveguide modes which survive above the original cut-off of the single ribbon (marked with crosses) and to which we refer subsequently as gap modes. These only exist for coupling strong enough to get a bonding cut-off at lower energy than the operation wavelength (as shown schematically in figure 3(b)), i.e. for small enough gaps.

Besides dispersion, the field distributions displayed by the modes discussed here vary considerably as well. For instance, the anti-bonding waveguide modes have an intense field right at the surface of the nanostructure, see figure 5(c), which could be highly beneficial for detection of surface modification such as binding events and so be of use in sensing schemes. In addition, these modes can propagate long enough for the changes in the plasmonic response to be measured electrically at the end of the ribbons. On the other hand, the field in bonding waveguide modes is tightly confined within the gap with this geometrical dimension being the main limitation to the confinement. The lateral spreading itself is just about a couple of nanometres and the propagation is slightly over a hundred nanometres, making nanocircuitry applications difficult. Most promising for integrated optics are the gap modes, which present a slightly different field profile than the bonding waveguide modes—with some field located close to the edges of the sandwich. Indeed these modes have a faster lateral decay than the latter, combined with a propagation about 50 times longer. Moreover and as we are going to show next, they also exist at the interface between a single ribbon and a conductor, such as a metallic substrate or a doped semiconductor. Last, some fascinating new physics could be uncovered in edge modes due to their singular dimensionality and extreme confinement. For gap small enough ($< \lambda_0/1000$) it is even possible to make ultra-narrow sandwiches (i.e. far below the cut-off width) where the four edges interact into a bonding combination (mode 4 in figures 5(a) and (b)) giving a field distribution mostly centred in the gap [40, 43]. This highly coupled hybridized mode could mark the limit of field confinement and plasmonic integration that could be ever reached.

3.4. Beyond graphene/air/graphene sandwiches

3.4.1. Graphene-conductor gap modes. One of the most attractive characteristics of graphene is the spectral tunability offered by doping, which shifts the Fermi level and therefore the range of frequencies in which plasmonic excitations can occur [23]. At a fixed wavelength, this means that doping will considerably increase the propagation length of the modes, as illustrated in figure 6 for the case of a sandwich (open triangles), but decrease the confinement.

Furthermore, changing the Fermi level affects the cut-offs of both the bonding and anti-bonding modes. Indeed for the case of $\mu = 1$ and 0.5 eV (above cut-off) there is no anti-bonding waveguide mode while they start appearing for $\mu = 0.2$ and 0.1 eV which have a sufficiently higher cut-off.

All nanostructures considered until this point where free-standing and spaced by air gaps which simplified discussion and understanding of the modes. Asymmetric dielectric environments were already investigated [40], with the conclusion that the physics of the hybridization was left largely unchanged by a modified surrounding. In particular, we observe that the bonding modes are mostly sensitive to the gap refractive index and that the effect of a substrate or a surrounding medium is very limited. However, anti-bonding modes, in which

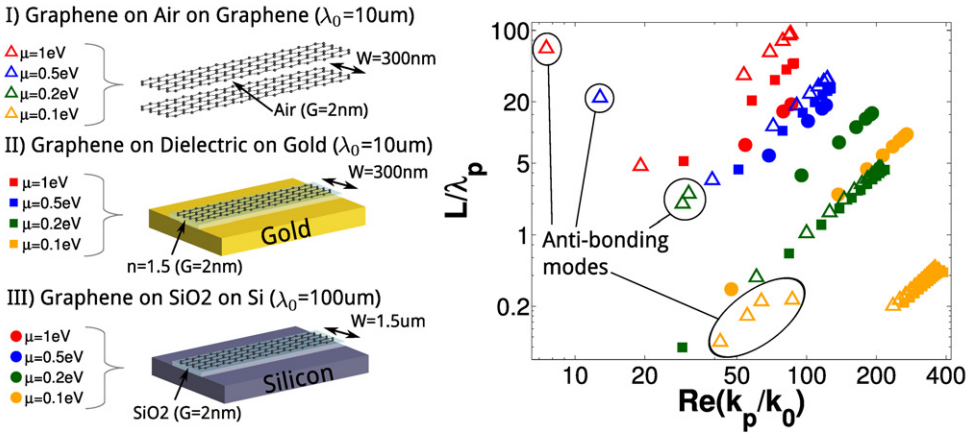

Figure 6. Mode spectra of (I) a graphene sandwich (open triangles) for different dopings (or chemical potentials μ) compared with (II) a graphene ribbon placed on top of a gold substrate spaced by a 2 nm thick dielectric spacer with refractive index $n = 1.5$ (full squares) and (III) a wider ribbon at $\lambda_0 = 100\,\mu$m on top of a silicon substrate coated with a 2 nm thick silica layer (full circles).

most of the field is located outside the gap, can completely disappear if the environment gets too asymmetric (not shown here). This makes these modes indeed very suitable for sensing modalities. The sandwich geometry even though very appealing for its performances could prove difficult to achieve experimentally. Hence we consider now simpler and more realistic configurations where a single ribbon is placed on top of a conducting substrate with a 2 nm dielectric spacer with refractive index $n = 1.5$. This geometry can easily be achieved by coating metals (for the visible and infrared regimes) or doped semiconductors (in the terahertz) with oxides or thin organic layers.

As a first example, we analyse the modes exhibited by a single graphene ribbon deposited on top of a gold substrate, see inset in figure 6. Along with the graphene sandwich discussed earlier, we vary the doping of the ribbon and plot the resulting spectra in figure 6 (full squares). Surprisingly, there are bonding modes with a metallic substrate as well and they are very similar to the case of the sandwich. For example, the two cases above cut-off ($\mu = 1$ and 0.5 eV) still exhibit gap modes. However, since gold in this regime acts mainly as a perfect conductor, the induced image charges have always the opposite sign of the ribbon plasmons thus preventing the creation of anti-bonding configuration for both the edge and waveguide modes. Last, a slight reduction of the propagation length can be noticed due to the asymmetric nature of the graphene-gold geometries compared with the graphene sandwiches.

Another very appealing system is to use a highly doped silicon substrate with a thin oxide layer for terahertz operation (here $\lambda_0 = 100\,\mu$m), as shown in the inset of figure 6. Since the free-space wavelength is substantially bigger than previous cases the width of the graphene ribbon is increased to $W = 1.5\,\mu$m in order to support waveguide modes. The spectra for this graphene/silica/silicon are plotted in figure 6 as full circles. The most striking observation is that the same modes are present with similar propagation within a 2 nm spacer while the wavelength is ten times larger than before. This represents an extraordinary confinement of $G/\lambda \sim 50\,000$. That such a dramatic compression can be reached is surprising

at first. However, one should remember that the modes are propagating in the horizontal plane. Therefore, the main property governing the interaction across the gap is the evanescent decay of the plasmons away from the graphene interface. In graphene, this decay is about a couple of nanometres compared to metals which display a decay length 10–100 times longer.

We foresee experimental demonstrations of the existence and manipulation of the gap modes in such simple geometries. Due to their remarkable confinement and long propagation they could be an ideal interface for integrated optics.

4. Conclusion

We analyse the physics of different kinds of guided modes in graphene nanoribbon sandwiches, and notice the emergence of strongly confined modes where the hybridization mediated by the interlayer spacing proves to be a powerful tool to modify the confinement and propagation length. The interaction between two graphene sheets gives rise to the formation of bonding and anti-bonding combinations of waveguide and edge modes of the single structure. Of particular interest are the anti-bonding waveguide modes which exhibit high field concentration at the external faces which can be used to probe the local environment in sensing schemes while electromagnetic waves experience an unprecedented squeezing in the waveguide bonding states. More attractive are the coupled modes which exist beyond the isolated ribbon cut-off as they can propagate longer while keeping extreme confinement. We finally demonstrate that these gap modes also exist at the interface between graphene ribbons and any conducting substrate. This allows to compress terahertz waves into 2 nm gaps reaching confinement of about five orders of magnitude. The use of semiconducting substrates promises an even greater control over and integration of these modes. In consequence, such a simple configuration could serve as building-blocks for tunable integrated optical components.

Acknowledgments

This work was sponsored by the EPSRC/NSF Materials World Network EP/H046887/1 and the Leverhulme Trust.

Appendix

A.1. Numerical method

The numerical results presented here were calculated using the commercial FEM package COMSOL considering infinitely long ribbons. The graphene is treated as an effective medium with a thickness $t = 0.5$ nm. This thickness was judged sufficiently thin since the results had converged for $t \leqslant 1$ nm and allowed to access fully converged results with reduced computation power. The conformal triangular meshing allowed element sizes $s = t/2$ to be used within the ribbon and the smallest gaps with a convergence as good as when $s = t/5$. The permittivity of the graphene was approximated by $\varepsilon = 1 + \mathrm{i}\sigma/\varepsilon_0\omega t$ as proposed in [4], where t is the effective thickness. The conductivity itself was described according to the local random phase approximation of the Kubo formula [44] which reads for finite temperature as $\sigma = \sigma_{\mathrm{intra}} + \sigma_{\mathrm{inter}}$

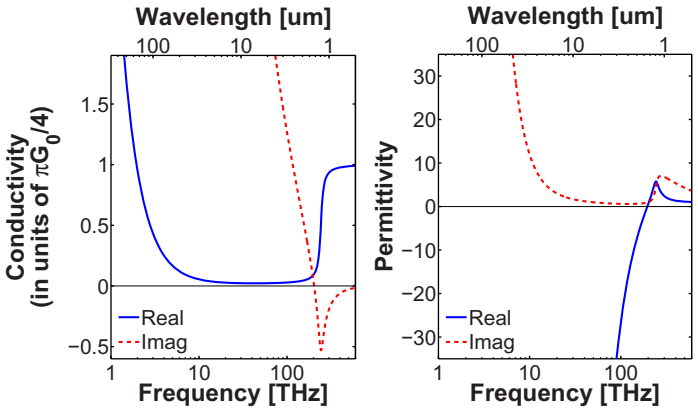

Figure A.1. Real and imaginary parts of the conductivity (left) and permittivity (right) for graphene at $T = 300\,\mathrm{K}$ with $\mu = 0.5\,\mathrm{eV}$ and $\Gamma = 0.1\,\mathrm{meV}$. The conductivity is given in units of $\pi G_0/4 = 6.08 \times 10^{-5}\,\mathrm{S}$ and the permittivity is calculated for an effective thickness of 0.5 nm.

with the interband and intraband contributions being

$$\sigma_{\mathrm{intra}} = \frac{2\mathrm{i}e^2 T}{\hbar^2 \pi (\omega + \mathrm{i}\Gamma)} \ln\left[2\cosh\left(\frac{\mu}{2T}\right)\right],$$

$$\sigma_{\mathrm{inter}} = \frac{e^2}{4\hbar}\left[\frac{1}{2} + \frac{1}{\pi}\arctan\left(\frac{\hbar\omega - 2\mu}{2T}\right) - \frac{\mathrm{i}}{2\pi}\ln\frac{(\hbar\omega + 2\mu)^2}{(\hbar\omega - 2\mu)^2 + (2T)^2}\right],$$

where T is the temperature energy, Γ the charge carriers scattering rate, μ the chemical potential (or Fermi level) and $\hbar\omega$ the photon energy. In all the calculations, $T = 300 \times k_{\mathrm{B}}$, $\mu = 0.5\,\mathrm{eV}$ and $\Gamma = 0.1\,\mathrm{meV}$ except in figure 6 where μ is varied from 0.1 to 1 eV. The real and imaginary parts of the conductivity (left) and permittivity (right) of such graphene are presented in figure A.1.

The optical properties of gold and silicon ($N = 1 \times 10^{20}\,\mathrm{cm}^{-3}$) were taken from experimental data [45, 46].

References

[1] Geim A K and Novoselov K S 2007 *Nature Mater.* **6** 183–91
[2] Castro Neto A H, Guinea F, Peres N M R, Novoselov K S and Geim A K 2009 *Rev. Mod. Phys.* **81** 109–62
[3] Geim A K 2009 *Science* **324** 1530–4
[4] Vakil A and Engheta N 2011 *Science* **332** 1291–4
[5] Bonaccorso F, Sun Z, Hasan T and Ferrari A C 2010 *Nature Photon.* **4** 611–22
[6] Avouris P 2010 *Nano Lett.* **10** 4285–94
[7] Bao Q and Loh K P 2012 *ACS Nano* **6** 3677–94
[8] Grigorenko A N, Polini M and Novoselov K S 2012 *Nature Photon.* **6** 749–58
[9] Giannini V, Berrier A, Maier S M, Antonio Sanchez-Gil J and Rivas J G 2010 *Opt. Express* **18** 2797–807
[10] Ng B, Hanham S M, Giannini V, Chen Z C, Tang M, Liew Y F, Klein N, Hong M H and Maier S A 2011 *Opt. Express* **19** 14653–61
[11] Berrier A, Albella P, Poyli M A, Ulbricht R, Bonn M, Aizpurua J and Rivas J G 2012 *Opt. Express* **20** 5052–60
[12] Hanham S M, Fernández-Domínguez A I, Teng J H, Ang S S, Lim K P, Yoon S F, Ngo C Y, Klein N, Pendry J B and Maier S A 2012 *Adv. Mater.* **24** OP226–30

[13] Liu H, Liu Y and Zhu D 2011 *J. Mater. Chem.* **21** 3335–45
[14] Wang F, Zhang Y, Tian C, Girit C, Zettl A, Crommie M and Shen Y R 2008 *Science* **320** 206–9
[15] Li Z Q, Henriksen E A, Jiang Z, Hao Z, Martin M C, Kim P, Stormer H L and Basov D N 2008 *Nature Phys.* **4** 532–5
[16] Ju L *et al* 2011 *Nature Nanotechnol.* **6** 630–4
[17] Fei Z *et al* 2012 *Nature* **487** 82–5
[18] Chen J *et al* 2012 *Nature* **487** 77–81
[19] Fang Z, Wang Y, Liu Z, Schlather A, Ajayan P M, Koppens F H L, Nordlander P and Halas N J 2012 *ACS Nano* **6** 10222–8
[20] Jablan M, Buljan H and Soljačić M 2009 *Phys. Rev.* B **80** 245435
[21] Fei Z *et al* 2011 *Nano Lett.* **11** 4701–5
[22] Zhou W, Lee J, Nanda J, Pantelides S T, Pennycook S J and Idrobo J C 2012 *Nature Nanotechnol.* **7** 161–5
[23] Koppens F H L, Chang D E and García de Abajo F J 2011 *Nano Lett.* **11** 3370–7
[24] Giannini V, Fernandez-Dominguez A I, Sonnefraud Y, Roschuk T, Fernandez-Garcia R and Maier S A 2010 *Small* **6** 2498–507
[25] Gao W, Shu J, Qiu C and Xu Q 2012 *ACS Nano* **6** 7806–13
[26] Manjavacas A, Nordlander P and García de Abajo F J 2012 *ACS Nano* **6** 1724–31
[27] Li P and Taubner T 2012 *ACS Nano* **6** 10107–14
[28] Yan H, Xia F, Li Z and Avouris P 2012 *New J. Phys.* **14** 125001
[29] Alaee R, Farhat M, Rockstuhl C and Lederer F 2012 *Opt. Express* **20** 28017–24
[30] Fallahi A and Perruisseau-Carrier J 2012 *Phys. Rev.* B **86** 195408
[31] Crassee I, Orlita M, Potemski M, Walter A L, Ostler M, Seyller T, Gaponenko I, Chen J and Kuzmenko A B 2012 *Nano Lett.* **12** 2470–4
[32] Yan H, Li Z, Li X, Zhu W, Avouris P and Xia F 2012 *Nano Lett.* **12** 3766–71
[33] Wang W, Apell S P and Kinaret J M 2012 *Phys. Rev.* B **86** 125450
[34] Wang B, Zhang X, García-Vidal F J, Yuan X and Teng J 2012 *Phys. Rev. Lett.* **109** 073901
[35] Liu P, Cai W, Wang L, Zhang X and Xu J 2012 *Appl. Phys. Lett.* **100** 153111
[36] Wang B, Zhang X, Yuan X and Teng J 2012 *Appl. Phys. Lett.* **100** 131111
[37] Fang Z, Thongrattanasiri S, Schlather A, Liu Z, Ma L, Wang Y, Ajayan P M, Nordlander P, Halas N J and Garcia de Abajo F J 2013 *ACS Nano* **6** 2388–95
[38] Nikitin A Y, Guinea F, García-Vidal F J and Martín-Moreno L 2011 *Phys. Rev.* B **84** 161407
[39] Berini P 2009 *Adv. Opt. Photon.* **1** 484–588
[40] Christensen J, Manjavacas A, Thongrattanasiri S, Koppens F H L and García de Abajo F J 2012 *ACS Nano* **6** 431–40
[41] Zia R, Selker M D and Brongersma M L 2005 *Phys. Rev.* B **71** 165431
[42] Halas N J, Lal S, Chang W S, Link S and Nordlander P 2011 *Chem. Rev.* **111** 3913–61
[43] Veronis G and Fan S 2007 *J. Lightwave Technol.* **25** 2511–21
[44] Nikitin A Y, Guinea F, García-Vidal F J and Martín-Moreno L 2011 *Phys. Rev.* B **84** 195446
[45] Palik E 1998 *Handbook of Optical Constants of Solids* vol 1 (New York: Academic)
[46] Spitzer W and Fan H Y 1957 *Phys. Rev.* **108** 268–71